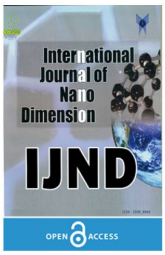

Volume 15, Issue 2, 152413 (1-12)

International Journal of Nano Dimension (IJND)

https://doi.org/10.57647/j.ijnd.2024.1502.13

DFT analyses of diamond-assisted paclitaxel anticancer conjugations and evaluating their features regarding the nano-based drug delivery approach

Newsha Saeedi[1], Ebrahim Balali[2*]

[1]*Department of Biology, Science and Research Branch, Islamic Azad University, Tehran, Iran.*
[2]*Department of Organic Chemistry, Faculty of Pharmaceutical Chemistry, Tehran Medical Sciences, Islamic Azad University, Tehran, Iran.*

[*]**Corresponding author:** ebrahim.balalii99@gmail.com

RESEARCH PAPER

Received:
12 December 2023
Revised:
18 January 2024
Accepted:
26 January 2024
Published online:
30 March 2024

Abstract:

Conjugations of a diamond (Diam) nanoflake and the paclitaxel (PTX) anticancer were investigated by analyzing the structural and electronic specifications obtained by density functional theory (DFT) regarding the nano-based drug delivery approach. The results indicated the formation of two physically interacting PTX@Diam conjugations; C1 and C2 with the strength values of -9.96 and -25.28 kcal/mol, respectively. The analyses of featured properties indicated an organizing role of Diam nanoflake for the next behaviors of PTX drug especially in the C2 conjugation. The localizations of all molecular orbital patterns were found at the surface of Diam nanoflake in both of C1 and C2 indicating its dominant role for managing the electronic behaviors. Additionally, chemical potential (-4.14 eV) of PTX was found better in C2 with a so much likely chemical potential (-4.28 eV) to the isolated PTX substance. Hereby, an enhanced PTX@Diam conjugated system was propped by this work regarding the nano-based drug delivery developmental approach.

Keywords: Anticancer; Computations; Drug delivery; Interactions; Nanocomposite

1. Introduction

Managing the health system levels of nowadays has been mainly affected by the wildness of current diseases and the appearance of new ones, in which several efforts have been dedicating to learn details of such complicated issues [1–3]. To overcome such problematic issues, either learning details of bio-related health systems or devolving novel therapeutic substances might lead to provide a higher level of treatment for the patients [4–6]. For approaching successful drug delivery platforms, nanostructures have been found as suitable substances of conjugations for enhancing the drug efficiencies by playing carrier and sensor roles [7, 8]. Based on the results of earlier works, benefits of making conjugated substances for improving the drug efficiency were identified through the formation of both of chemical and physical conjugated systems [9, 10]. Accordingly, the efforts of researchers leaded to the initiation of nano drug delivery systems to manage the process in a targeted route for enhancing the patients' treatment efficiency [11, 12]. It is important to remind that the developments of so many types of bio-related materials are still required for successfully dealing with the human living systems [13–15]. Because of appropriate structural and electronic features, nanostructures have been always expected to work as good complementary substances for contributing to several reactions and interactions [16–19]. To this time, considerable research works have been done to indicate benefits of nanostructures for interacting with the drug substances to optimize their functions towards a specific treatment process [20, 21]. Accordingly, the characteristic features of such conjugated systems have been found by the results of structural and electronic analyses emphasizing on the managing and controlling role of nanostructures for determining the next functions of drug substances [22, 23]. Hereby, the nano-based drug delivery processes have been focused by considerable research works up to now for customizing the nano-drug conjugated systems [24, 25]. To this aim, learning the detailed infor-

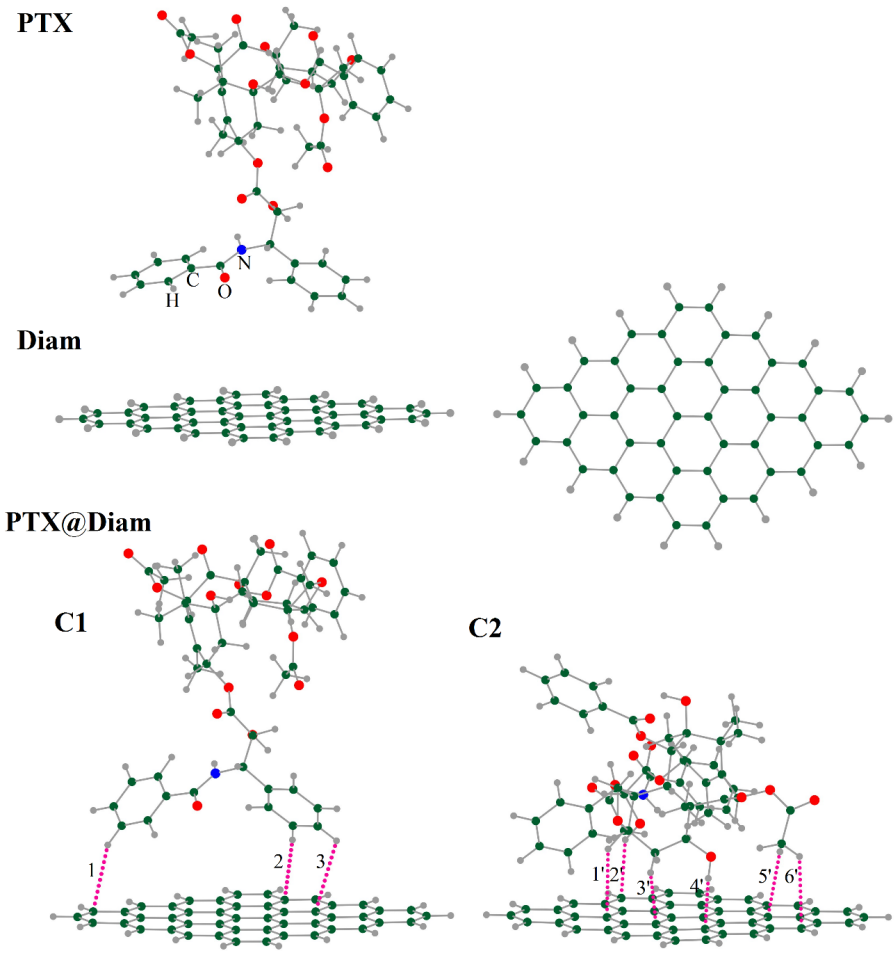

Figure 1. Structural representation of PTX (Paclitaxel), Diam (Diamond nanoflake), C1 and C2 (Conjugated PTX@Diam) models; interactions in the conjugated C1 and C2 models were shown in dot-lines.

mation between drug and nanostructure counterparts are essential, in which the computational tools are very useful for providing the required insights and information [26–28]. Nanostructures have been firstly introduced by the pioneering carbon nanotube; however, several other forms and structures have been characterized for these novel materials [29–32]. The characteristic structural and electronic features of nanostructures have proposed them as unique materials for working in different purposes and applications [33, 34]. Indeed, a need of developing novel materials for the biomedical purposes emerged considerable investigations on the materials characterizations towards working in the bio-related systems [35, 36]. To this aim, several efforts were done to recognize the specific materials for the specific purposes [37, 38]. For the case adsorption or carrier processes, a stable nanostructure is needed for approaching a stable conjugated system between the interacting counterparts [39, 40]. To this aim, a diamond-like model was investigated in the current research work to be conjugated with the paclitaxel anticancer regarding the nano-based drug delivery approach. Diamond (Diam) has been also categorized among the nanostructures within a stable nanoflake configuration as reported by the earlier research works [41, 42]. Accordingly, the surface of such a stable Diam nanoflake was used in this work towards an anticancer (Figure 1) to customize the formation of a conjugated system for proposing a possible drug delivery platform.

Paclitaxel (PTX), or Taxol, is a known anticancer drug for chemotherapy of various cancers involving breast, lung, cervical, ovarian, esophageal, and pancreatic ones [43–47]. Although PTX is working among the suitable medications, but allergic reaction, numbness, bone marrow suppression, muscle pain, and hair loss have been observed as side effects for the patients [48–52]. Hence, improving the medication efficiency of PTX has been focused by several works up to now and further investigations are still required to approach a more successful level of medication [53–57]. By the supposed roles of nanostructures for working as carriers of drug delivery processes, a conjugated system of interacting PTX and Diam counterparts was explored within the current work along with density functional theory (DFT) calculations. Both of isolated and conjugated systems of investigating models were analyzed in to determine details of structural interactions and the post-conjugation features. Figures 1-4 exhibited the structural interacting counterparts and mechanism of conjugations and the related graphical electronic features. Tables 1-3 included the quantitative structural and electronic specifications of the models. The structural analyses of diamond-assisted paclitaxel anticancer conjugations (PTX@Diam) and evaluating their features

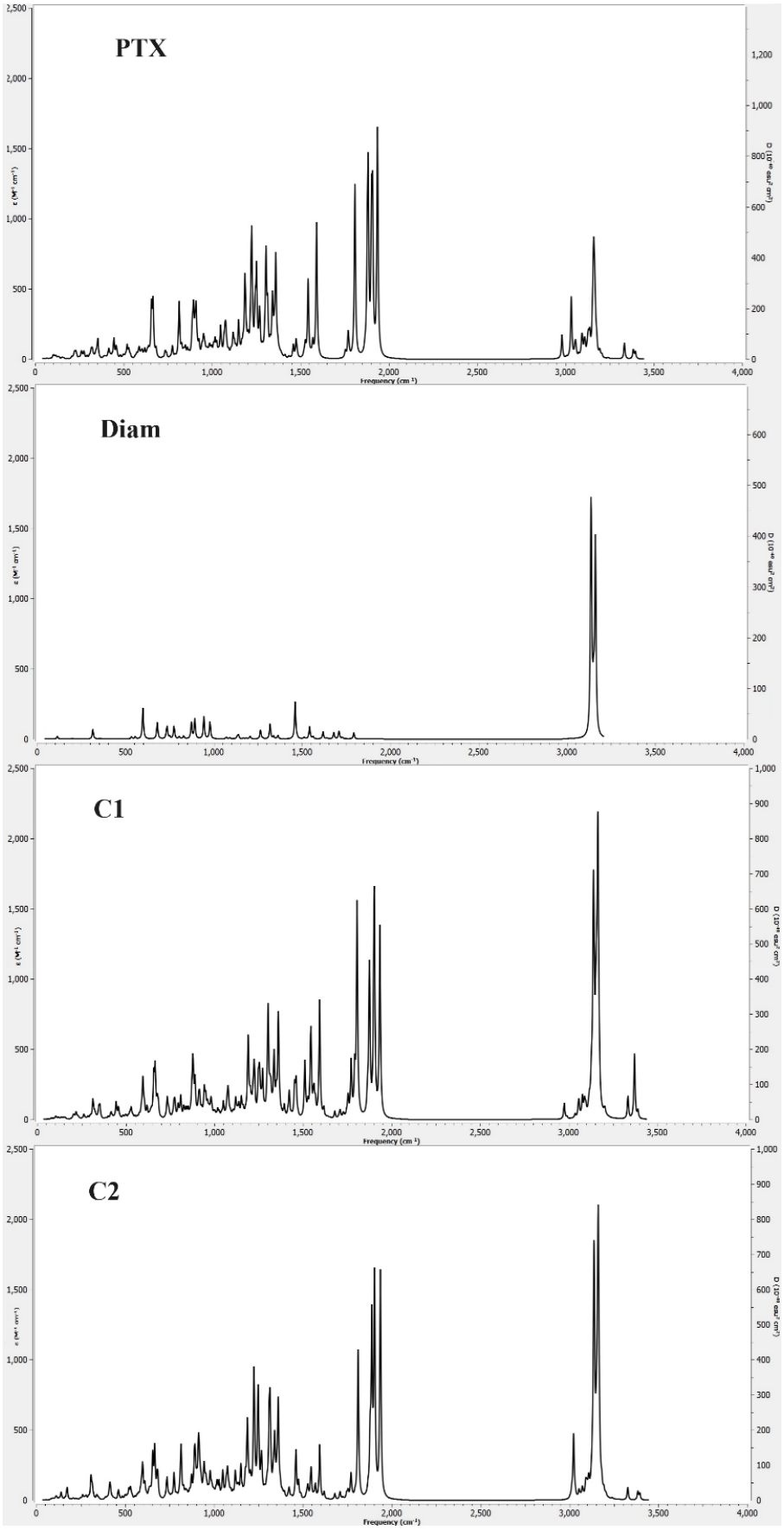

Figure 2. Infrared (IR) spectra representation of PTX, Diam, and C1 and C2 conjugated PTX@Diam models.

Table 1. Structural specifications of C1 and C2 conjugated PTX@Diam models.

Model	ε (kcal/mol)	**PTX**$\cdots$**Diam**	**d** ($\AA$)	ρ (au)	$\nabla^2\rho$ (au)	**H** (au)
C1	-9.96	1: H$\cdots$C	3.08	0.0039	0.0123	0.0007
		2: H$\cdots$C	3.11	0.0036	0.0115	0.0006
		3: H$\cdots$C	3.34	0.0025	0.0084	0.0004
C2	-25.28	1′: H...C	3.01	0.0044	0.0147	0.0008
		2′: H$\cdots$C	2.57	0.0087	0.0284	0.0012
		3′: H$\cdots$C	2.52	0.0108	0.0358	0.0013
		4′: H$\cdots$C	2.27	0.0151	0.0468	0.0076
		5′: H$\cdots$C	3.17	0.0032	0.0106	0.0006
		6′: H$\cdots$C	3.19	0.0034	0.0106	0.0005

along with the DFT calculations was the main idea of this work to provide information for developing nano-based drug delivery approach.

2. Computational methods

This molecular scale work was done based on DFT calculations, which were performed using the Gaussian 09 D.01 program employing the dispersion effect corrected wB97XD functional and the 6-31G* bases set [58–60]. Indeed, the current research works was done by the benefits of employing computational tools for investigating the features properties of chemical systems [61, 62]. Hereby, the investigated models involved the 3D structures of isolated forms of PTX and Diam and physically interacting PTX@Diam conjugations; C1 and C2 (Figure 1). The geometries of isolated and conjugated models were stabilized by performing optimization calculations and involving interactions were extracted using the Multiwfn 3.8 program based on the quantum theory of atoms in molecules (QTAIM) analyses [63, 64]. Additionally, the vibrational frequencies were calculated and corresponding Infrared (IR) spectra were exhibited in Figure 2. Moreover, the impacts of water solvent on the thermochemistry features of conjugated systems were recognized (Table 2) by implementing the water solvent based on polarizable continuum model (PCM) method [65]. At this point of investigation, the structural specifications were found and the energies (E) were evaluated to recognize the strength of conjugated systems (ε) through eq. (1) besides the evaluated QTAIM features (Table 1). For avoiding any overestimation of energies, the impacts of basis set superposition error (BSSE) [66] were considered in the evaluation of ε values. Additionally, variations of thermochemistry features for Gibbs free energy (G), enthalpy (H), and entropy (S) of conjugated systems in gas and water phases were recognized using eqs. (2)-(4).

$$\varepsilon = E_{PTX@Diam} - E_{PTX} - E_{Diam} + BSSE \quad (1)$$

$$\Delta G_{Water-Gas} = \Delta G_{Water} - \Delta G_{Gas} \quad (2)$$

$$\Delta H_{Water-Gas} = \Delta H_{Water} - \Delta H_{Gas} \quad (3)$$

$$\Delta S_{Water-Gas} = \Delta S_{Water} - \Delta S_{Gas} \quad (4)$$

Next, the models were characterized by performing frontier molecular orbital (FMO) calculations [67, 68] on the optimized systems, in which the results were divided into two parts; the graphical representations of Figures 3 and 4 and the quantitative features of Table 3. At this point of investigation, both of qualitative and quantitative electronic specifications of models were known. Energy levels of the highest occupied molecular orbital (HOMO) and the lowest unoccupied molecular orbital (LUMO) of dominant FMO levels were extracted directly and eqs. (5) – (8) were used for obtaining their related features [69, 70]. Accordingly, Table 3 included the obtained values of energy gap (δ), chemical potential (μ), chemical hardness (η), and charge transfer (Q). Additionally, the values of dipole moments (μ_d) were also included in Table 3. Figure 3 exhibited the graphical representations of HOMO and LUMO distribution patterns as evaluated by the Chemcraft 1.8 program [71] and Figure 4 exhibited the diagrams of density of states (DOS) as evaluated by the GaussSum 3.0 program [72].

$$\delta = E_{LUMO} - E_{HOMO} \quad (5)$$

$$\mu = \frac{1}{2}(E_{LUMO} + E_{HOMO}) \quad (6)$$

$$\eta = \frac{1}{2}(E_{LUMO} - E_{HOMO}) \quad (7)$$

$$Q = Q_{DiaminPTX@Diam} - Q_{Diam} \quad (8)$$

3. Results and discussion

The current research work was done by the importance of developing nano-based systems for approaching successful drug delivery processes, in which the topic requires further investigations to provide more detailed insights and information [73–75]. To the point, the main goal of this work was considered to focus on the assessment of benefits of a representative diamond surface (Diam) to adsorb the Paclitaxel (PTX) drug along with the formation PTX@Diam conjugations. The employed method was DFT calculations and the models and their evaluated results were exhibited in Figures 1-4 and Tables 1-3. Indeed, the main novelty of this work was focusing on the determination of involving interactions inside the PTX@Diam conjugated systems and to show the benefits of such a conjugated model regarding the evaluated structural and electronic properties. Hereby, the achievements were discussed by the following parts structural specifications and electronic specifications.

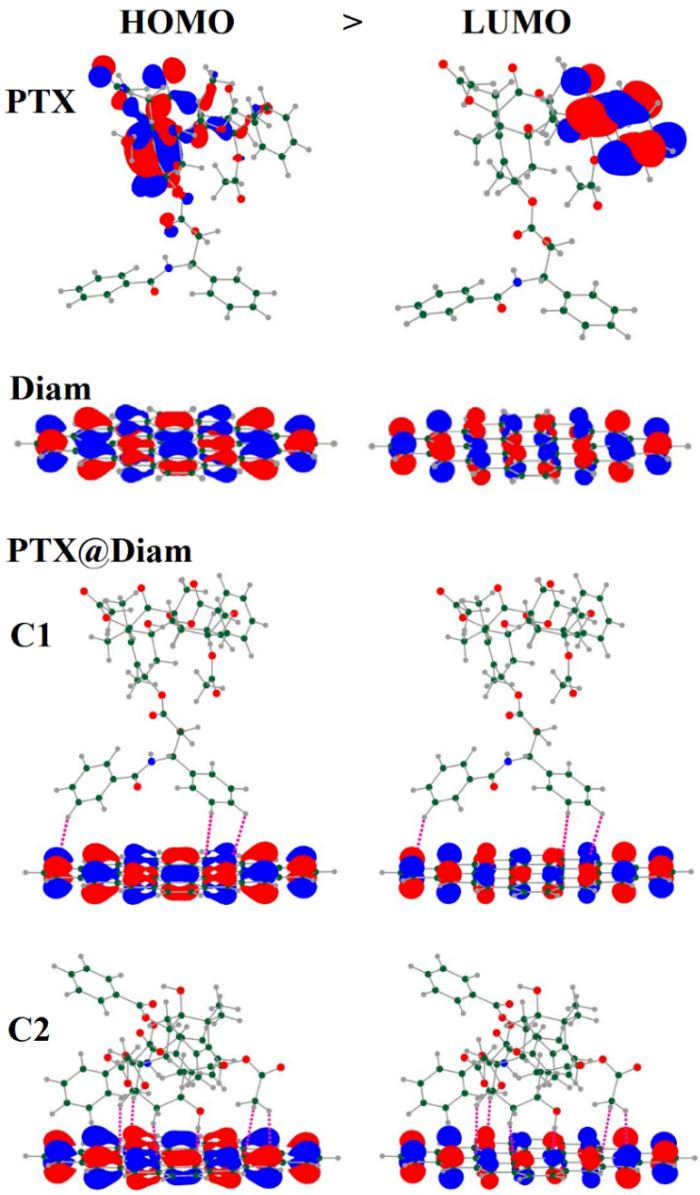

Figure 3. Electronic HOMO and LUMO distribution pattern representation of PTX, Diam, and C1 and C2 conjugated PTX@Diam models.

Indeed, the experimental investigations are essential to recognize the availability of chemical systems; however, so many types of detailed insights and information could be learned by computational investigations [76].

3.1 Structural specifications

The model structures were shown in Figure 1 including the isolated PTX and Diam and their physically interacting PTX@Diam conjugations; C1 and C2. The models were finalized by optimizing the geometries of both of isolated and conjugated systems. Their stabilities were also examined by performing additional calculations of vibrational frequencies avoiding the existence of any imaginary frequency, in which the evaluated IR spectra were exhibited in Figure 2. To further analysis the details of existing interactions, the QTAIM based analyses were performed to identify the interactions and their specifications in the conjugated models. The Diam nanoflake was found as a planar system to adsorb the PTX drug substance, in which the formations of two conjugations were confirmed after examining all possible starting configurations for the PTX to contribute to interactions with the Diam surface. It should be reminded that the variations of initial orientations of PTX towards the surface of Diam were monitored carefully based on the achievement of energy convergence of optimization calculations. As a result, two configurations of conjugated systems were found stable to be investigated in this work as the most possible and available configurations of PTX@Diam conjugations. Hence, the models were assessed by the obtained energies, frequencies, and QTAIM properties as essential features of this work for assessing the structural specifications of the investigated models. Besides, the impacts of water solvent on the thermochemistry features of complexes were also examined and the results were summarized in Table 2. Ac-

cordingly, the featured properties of Tables 1 and 2 were obtained for discussing the conjugated systems formations and specifications.

In accordance with the results of Table 1, the obtained conjugation strengths (ε) indicated different modes of stabilities for the investigated models, in which the strength of C1 was found -9.96 kcal/mol and that of C2 was found -25.28 kcal/mol. Hence, the ε quantity indicated a reasonable strength of conjugation for both of C1 and C2 systems, but with a higher suitability of conjugated systems formation for C2. The reasonability of conjugation was claimed because of obtaining a negative value of ε for both of conjugated systems, but with a higher strength for C2 rather than C1. Additionally, the obtained conjugated systems were found to be in a physical mode of interactions yielding a non-covalent formation of C1 and C2. This type of non-covalent formation could be related to the reversibility of conjugated systems to be involved in the drug delivery processes to be able to deliver their uploaded drug. Returning to Figure 1, it could be seen that the orientation of PTX towards the Diam surface is different in C1 and C2; hence, the models detected different environment of interactions for the formation of PTX@Diam conjugations. Beside a larger number of involving interactions in C2, the counterparts were located in a closer distance to each other as indicated by the d quantity. The performed QTAIM analyses identified the existence of one H···C interaction type from the PTX substance to the Diam nanoflake, but with different number of involving interactions in C1 and C2. In this case, an average value of 3.18 $\AA$ was fond for d of C1 and an average value of 2.79 $\AA$ was fond for d of C2. These values of d could affirm the existence of a physical conjugation system based on the formation of H···C interactions in both of C1 and C2, in which a very shorter d is needed for the formation of H-C chemical bond.

The remarkable features of QTAIM analyses including ρ, $\nabla^2\rho$, and H, indicated the role of each interaction in the conjugated systems, in which the results showed small portion of electron density for the interactions and the positive sign of H could re-affirm the existence of physically conjugated systems. However, comparing the interactions inside each conjugated system could reveal a characteristic role for each of interaction between the interacting atoms of two substances of PTX and Diam, In this case, although the interactions were mainly based on the formation of H···C interactions, but the total strength yielded a meaningful strength of PTX@Diam conjugation formation. For a conclusion; the formation of physically interacting PTX@Diam conjugated systems was affirmed by the obtained values of energies, interactions, distances, and QTAIM specifications while C2 was stronger than C1. Analyzing the evaluated IR spectra (Figure 2) also affirmed the formation of PTX@Diam conjugated systems, in which the changes of peaks from the regions of individual PTX and Diam to the conjugated systems were notable. Among the conjugated systems, comparisons of peaks also indicated an ability of distinguishing the conjugated systems from each other based on the evaluated IR specifications. The corresponding evaluated thermochemistry features (Table 2) also indicated

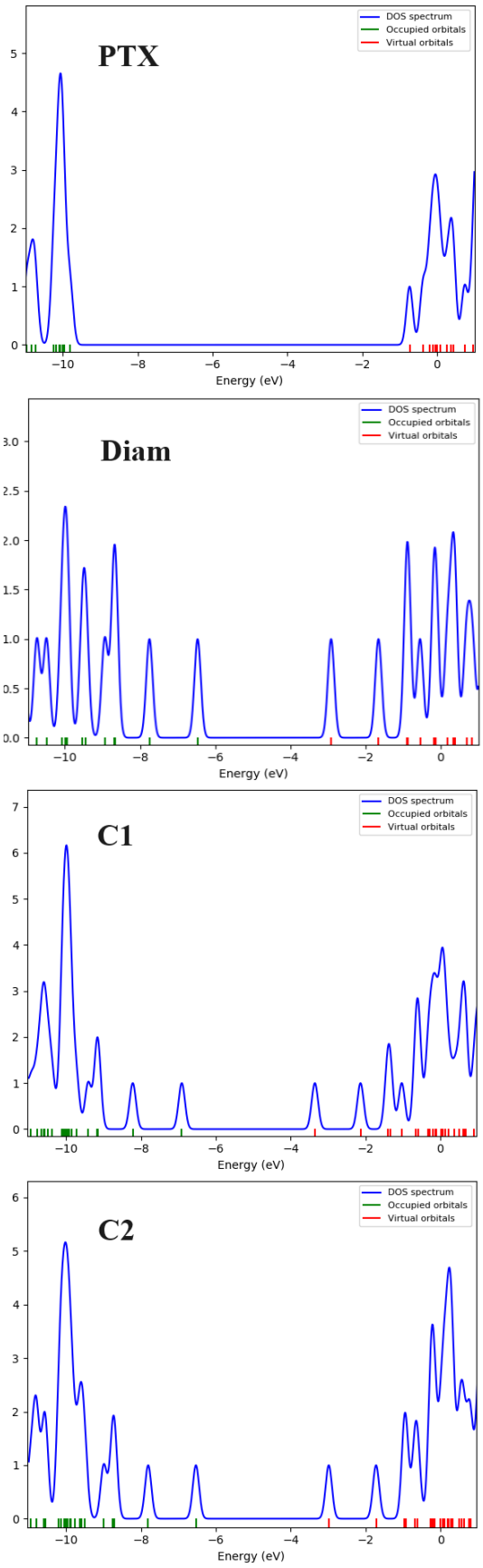

Figure 4. Density of states (DOS) diagram representation of PTX, Diam, and C1 and C2 conjugated PTX@Diam models.

Table 2. Impacts of water solvent on the thermochemistry features of C1 and C2 conjugated PTX@Diam models.

Model	$\Delta G_{Water-Gas}$	$\Delta H_{Water-Gas}$	$\Delta S_{Water-Gas}$
C1	-10.52	-10.29	2.74
C2	-15.06	-14.81	5.23

the availability of conjugated systems in the water phase even better than the gas phase. Indeed, the PTX counterpart itself played a good role of maintaining the structures in the water systems. Accordingly, the existence of water solvent helped to achieve better values for ΔG, ΔH, and ΔS, for the conjugated systems with the priority of C2 in comparison with C1. In this regard, the availability of the investigated models in water systems could be considered by the importance of watery environment of most of biological systems and drug delivery process. Hence, the models were stabilized based on reasonable features of structural specifications, in which the level of formation and strength could be also compared to earlier parallel works on the drug delivery processes [8, 56] revealing the reasonability of the results of current work for proposing the PTX@Diam conjugated systems as possible platforms of drug delivery process.

3.2 Electronic specifications

Besides the very important structural specifications analyses of chemical systems, electronic specifications analyses are crucial for determining the behaviors of chemical subsystems and their detectability. To this aim, analyzing the FMO related features could lead to the generation of insightful information about the systems. In this regard, the graphical representations of distribution patterns of dominant HOMO and LUMO levels of FMO were visualized for the isolated and conjugated systems (Figure 3). First of all, different localizations of HOMO and LUMO distribution patterns were found for the isolated PTX model, in which the interacting site of PTX in the formation of C2 was that side of HOMO and LUMO involvement while the interacting side of PTX in the formation of C1 was free of any localization. Accordingly, a stronger formation of C2 than C1 was expected regarding the closer distance of HOMO and LUMO patterns of C2 to the Diam surface than C1 to be involved in charge transferring process. The higher strength of C2 than C1 was already found by the structural specifications analyses. Next, a remarkable role of Diam nanoflake was found by adsorbing all the distribution patterns of conjugated systems at the surface of nanoflake and making the PTX substance free of any distribution pattern localization. Exactly at this point, the charge transfer direction was found from the PTX substance to the Diam nanoflake surface, in which the obtained value of Q was found to be -0.09 and -0.12 $|e|$ for C1 and C2 (Table 3). A major role of electron transferring the Diam nanoflake surface was found for C2 more significant that C1. As mentioned earlier, the conjugated systems are expected to work as enhanced platforms for approaching more targeted drug delivery processes by providing a controlling role of nanoflake carrier; the modes indicated a remarkable role for the Diam nanoflake to organize the electronic behavior of C1 and C2.

The electronic specifications of models (Table 2) were assessed further regarding the featured properties of characteristic EHOMO and ELUMO quantities and their related quantities including δ, μ, and η. Besides the mentioned achievement of Q and also distribution patterns localizations for the electron transferring processes, a possibility of electron transferring could be also recognized in the molecular models by the EHOMO and ELUMO quantities. Moreover, the evaluated values of μ_d showed significant changes of dipole moment quantity from the individual models to the conjugated systems. In both cases of conjugations, the dipole moment was increased regarding the individual PTX substance. Additionally, the individual Diam with $\mu_d = 0$ Debye reached to a polar level addressing a lower toxicity of Diam in the conjugated system in comparison with the individual form. The earlier results of water impacts also indicated a better stability of conjugated systems in the water phase, re-addressing to a lower toxity of conjugated systems. In the case of FMO analyses, lower or higher levels of HOMO and LUMO could determine the mechanism of electron transferring process as could be found by the variations of levels from the individual models to the conjugated systems. The new HOMO and LUMO levels of conjugated systems were closer to the old levels of isolated Diam nanoflake than those of isolated PTX substance. In this regard, the achievement of adsorbing all the distribution patterns for localizing at the Diam nanoflake surface was confirmed; as it was observed by the graphical representations of Figure 3. Moreover, a closer distance of HOMO and LUMO levels (δ) was found in the conjugated systems in comparison with the isolated PTX substance more similar to the distance in the isolated Diam nanoflake. These achievements could show the significant impacts of Diam

Table 3. Electronic specifications of PTX, Diam and C1 and C2 conjugated PTX@Diam models.

Model	E_{HOMO} (eV)	E_{LUMO} (eV)	δ (eV)	μ (eV)	η (eV)	**Q** $\|e\|$	μ_d (Debye)
PTX	-8.72	0.16	8.88	-4.28	4.44	–	10.45
Diam	-5.29	-2.10	3.19	-3.70	1.59	–	0
C1	-5.38	-2.18	3.20	-3.78	1.60	-0.09	10.66
C2	-5.78	-2.49	3.29	-4.14	1.64	-0.12	11.85

nanoflake for organizing the electronic behavior of conjugated systems, and the behavior of PTX indeed. The values of δ quantity was found as 3.20, 3.29, 3.19, and 8.88 eV for C1, C2, Diam, and PTX models, respectively. As the value of δ quantity increases, the value of η quantity also increases, as could be found by a large value for PTX (4.44 eV) in comparison with a smaller values of Diam (1.59 eV), C1 (1.60 eV), and C2 (1.64 eV). As the strength of C1 was lower than that of C2, a lower hardness was also found for C1 in comparison with C2. However, the value of μ quantity for C2 was found more likely to that of the isolated PTX showing the maintenance of electronic nature of PTX. It is indeed a challenging area that the conjugation of drug substances with other substances could lead to the change of their own featured properties, here within the obtained results, it could be learned that the changes are happening but the final results are mostly likely to each other in C2 and PTX. Indeed, the main benefit of running a detailed investigation is approaching more insights about the nature of investigating systems and evaluating their required information regarding the developmental issues.

3.3 Combinations of structural and electronic specifications

Careful analyses of structural and electronic specifications of isolated PTX and Diam and their PTX@Diam conjugated systems indicated a suitability of C2 for the formation of conjugated system by assessing the evaluated featured properties. However, the formation of both conjugated systems was accessible and reasonable regarding the magnitudes of energy strengths and involving interactions. Besides, the evaluated electronic features indicated a managing role of Diam nanoflake surface for the formation of both of C1 and C2 conjugated systems, but with a priority of C2 conjugation. The existence of non-covalent and physical interactions leaded to the formation of both of C1 and C2 conjugated systems in a suitable level of strength. On the other hand, more changes of FMO featured properties were indicated by the electronic quality and quantity and the values of μ quantity of C2 and the isolated PTX showed maintenance of electronic features of drug substance in the conjugated system, but under the Diam nanoflake organizing. Accordingly, the structural and electronic specifications confirmed the beneficial PTX@Diam conjugated systems by focusing the characteristic role of Diam nanoflake surface for the formation of conjugated systems especially by adsorbing the transferred charges of conjugated systems from the PTX counterpart.

4. Conclusions

Structural and electronic analyses of diamond-assisted (Diam) paclitaxel (PTX) anticancer conjugations (PTX@Diam) were done in this work along with DFT approach. Our results indicated the formations of two conjugated systems; C1 and C2, by the involvement of H$\cdots$C physical interactions between the PTX and Diam substances. The Diam nanoflake surface showed a remarkable role for organizing the conjugated systems, in which the featured properties indicated an advantage for formation of such conjugated systems for enhancing the drug behavior under a controlling system. The isolated PTX showed a very large value of chemical hardness quantity, in which it was decreased in the conjugated systems. Additionally, a remarkable role of Diam nanoflake was found regarding the electronic properties as the distribution patterns were all localized at the Diam surface in both of C1 and C2. As a highlighted achievement; the Diam nanoflake surface was found useful for enhancing the behavior of PTX drug under the organizing and controlling role of Diam nanoflake for determining the next behavior of PTX in the conjugated system. Indeed, the evaluated structural and electronic featured properties revealed a controllable situation of PTX drug among the PTX@Diam conjugated system under the Diam nanoflake surface administration.

Ethical Approval
This manuscript does not report on or involve the use of any animal or human data or tissue. So the ethical approval does not applicable.

Funding
No funding was received to assist with conducting this study and the preparation of this manuscript.

Authors Contributions
All authors have contributed equally to prepare the paper.

Availability of Data and Materials
The data that support the findings of this study are available from the corresponding author upon reasonable request.

Conflict of Interests
The authors declare that they have no known competing financial interests or personal relationships that could have appeared to influence the work reported in this paper.

References

[1] S. Karreinen, H. Paananen, L. Kihlström, K. Janhonen, M. Huhtakangas, M. Viita-Aho, and L.K. Tynkkynen. Living through uncertainty: A qualitative study on leadership and resilience in primary healthcare during COVID-19. *BMC Health Services Res*, **23**:233–237, 2023. DOI: https://doi.org/10.1186/s12913-023-09223-y.

[2] S. Eslami, N. Hosseinzadeh Shakib, Z. Fooladfar, S. Nasrollahian, S. Baghaei, S.A. Mosaddad, and M. Motamedifar. The role of periodontitis-associated bacteria in Alzheimer's disease: A narrative review. *J. Basic Microbiol*, **63**:1059–1064, 2022. DOI: https://doi.org/10.1002/jobm.202300250.

[3] A.K.O. Aldulaimi, S.S.S.A. Azziz, Y.M. Bakri, M.A. Nafiah, K. Awang, S. Aowda, M. Litaudon, N.M. Hassan, H. Naz, P. Abbas, and Y.Z.H. Hashim. Alkaloids from Alphonsea Elliptica Barks and their biological activities. *J. Global Pharma. Technol*, **10**:270–275, 2018. URL http://irep.iium.edu.my/68590.

[4] G. Dicuonzo, F. Donofrio, A. Fusco, and M. Shini. Healthcare system: Moving forward with artificial intelligence. *Technovation*, **120**:102510, 2023. DOI: https://doi.org/10.1016/j.technovation.2022.102510.

[5] S.A. Mosaddad, B. Rasoolzade, R.A. Namanloo, N. Azarpira, and H. Dortaj. Stem cells and common biomaterials in dentistry: A review study. *J. Mater. Sci*, **33**:55–61, 2022. DOI: https://doi.org/10.1007/s10856-022-06676-1.

[6] H.T. Mohammed, K.K. Alasedi, R. Ruyid, S.A. Hussein, A.L. Jarallah, S.M.A. Dahesh, M.Q. Sultan, Z.N. Salman, B.S. Bashar, A.K.O. Aldulaimi, and M.A. Obaid. ZnO/Co_3O_4 nanocomposites: Novel preparation, characterization, and their performance toward removal of antibiotics from wastewater. *J. Nanostruct*, **12**:503–509, 2022. DOI: https://doi.org/10.22052/JNS.2022.03.003.

[7] Y. Yang, S. Wang, P. Ma, Y. Jiang, K. Cheng, Y. Yu, N. Jiang, H. Miao, Q. Tang, F. Liu, and Y. Zha. Drug conjugate-based anticancer therapy-current status and perspectives. *Cancer Lett*, **552**:215969, 2023. DOI: https://doi.org/10.1016/j.canlet.2022.215969.

[8] M. Nezamabadi, E. Balali, and M. Qomi. A sumanene-chitosan scaffold for the adsorption of niraparib anticancer: DFT insights into the drug delivery. *Inorg. Chem. Commun*, **155**:111098, 2023. DOI: https://doi.org/10.1016/j.inoche.2023.111098.

[9] W. Liu, Z. Ma, Y. Wang, and J. Yang. Multiple nano-drug delivery systems for intervertebral disc degeneration: Current status and future perspectives. *Bioact. Mater*, **23**:274–278, 2023. DOI: https://doi.org/10.1016/j.bioactmat.2022.11.006.

[10] S.M.H. Hosseini, M.R. Naimi-Jamal, and M. Hassani. Preparation and characterization of mebeverine hydrochloride niosomes as controlled release drug delivery system. *Chem. Methodol*, **6**:591–596, 2022. DOI: https://doi.org/10.22034/CHEMM.2022.337717.1482.

[11] M.S. Jabar and S.A.W. Al-Shammaree. Cytotoxicity and anticancer effect of chitosan-ag nps-doxorubicin-folic acid conjugate on lungs cell line. *Chem. Methodol*, **7**:1–6, 2023. DOI: https://doi.org/10.22034/CHEMM.2023.359769.1604.

[12] M. Manuel and A. Jennifer. A review on starch and cellulose-enhanced superabsorbent hydrogel. *J. Chem. Re*, **5**:183–187, 2023. DOI: https://doi.org/10.22034/JCR.2023.382452.1209.

[13] M. Naeimi Darestani, B. Houshmand, S.A. Mosaddad, and M. Talebi. Assessing the surface modifications of contaminated sandblasted and acid-etched implants through diode lasers of different wavelengths: An in vitro study. *Photobiomodul. Photomed. Laser Surg*, **41**:201–207, 2023. DOI: https://doi.org/10.1089/photob.2023.0009.

[14] N. Musa, M. Sallau, A. Oyewale, and T. Ali. Bioactive compounds and antischistosomal activity of dolichos species: A review. *J. Chem. Rev*, **5**:416–420, 2023. DOI: https://doi.org/10.22034/JCR.2023.407571.1233.

[15] S.A. Mosaddad, A. Hussain, and H. Tebyaniyan. Green alternatives as antimicrobial agents in mitigating periodontal diseases: A narrative review. *Microorgan*, **11**:1269–1275, 2023. DOI: https://doi.org/10.3390/microorganisms11051269.

[16] M.J. Saadh, M. Mirzaei, S.M. Dhiaa, L.R. Hosseini, G. Kushakova, M. Da'i, and M.M. Salem-Bekhit. Density functional theory assessments of an iron-doped graphene platform towards the hydrea anticancer drug delivery. *Diam. Relat. Mater*, **141**:110683, 2024. DOI: https://doi.org/10.1016/j.diamond.2023.110683.

[17] A.O. Flayyih, W.K. Mahdi, Y.I.M. Abu Zaid, and F.H. Musa. Biosynthesis, characterization, and applications of bismuth oxide nanoparticles using aqueous extract of beta vulgaris. *Chem. Methodol*, **6**:620–626, 2022. DOI: https://doi.org/10.22034/CHEMM.2022.342124.1522.

[18] S.A. Jasim, H.H. Kzar, R. Sivaraman, M.J. Jweeg, M. Zaidi, O.K.A. Alkadir, F. Safaa Fahim, A.K.O. Aldulaim, and E. Kianfar. Engineered nanomaterials, plants, plant toxicity and biotransformation: A review. *Egypt. J. Chem*, **65**:151–156, 2022. DOI: https://doi.org/10.21608/ejchem.2022.131166.5775.

[19] S. Abdullaev, N.R. Barakayev, B.S. Abdullaeva, and U. Turdialiyev. A novel model of a hydrogen production in micro reactor: Conversion reaction of methane with water vapor and catalytic. *Int. J. Thermofluid*, **20**:100510, 2023. DOI: https://doi.org/10.1016/j.ijft.2023.100510.

[20] M.M. Salem-Bekhit, M. Da'i, M.M. Rakhmatullaeva, M. Mirzaei, S. Al Zahrani, and N.A. Alhabib. The drug delivery of methimazole through the sensing function assessments of BeO fullerene-like particles: DFT study. *Chem. Phys. Impact*, **7**:100335, 2023. DOI: https://doi.org/10.1016/j.chphi.2023.100335.

[21] E. Balali, S. Sandi, M. Sheikhi, S. Shahab, and S. Kaviani. DFT and TD-DFT study of adsorption behavior of Zejula drug on surface of the $B_{12}N_{12}$ nanocluster. *Main Group Chem*, **21**:405–411, 2022. DOI: https://doi.org/10.3233/MGC-210120.

[22] D. Ezhilarasan, T. Lakshmi, and S. K. Mallineni. Nano-based targeted drug delivery for lung cancer: Therapeutic avenues and challenges. *Nanomedicine*, **17**:1855–1862, 2022. DOI: https://doi.org/10.2217/nnm-2021-0364.

[23] M.J. Ansari, M.F. Aldawsari, A. Zafar, A. Soltani, M. Yasir, M.A. Jahangir, M. Taleuzzaman, V. Erfani-Moghadam, L. Daneshmandi, N.O. Mahmoodi, and A. Yahyazadeh. In vitro release and cytotoxicity study of encapsulated sulfasalazine within LTSP micellar/liposomal and TSP micellar/niosomal nanoformulations. *Alexandria Eng. J*, **61**:9749–9754, 2022. DOI: https://doi.org/10.1016/j.aej.2022.02.019.

[24] A. Gholami, E. Shakerzadeh, and E.C. Anota. Exploring the potential use of pristine and metal-encapsulated $b_{36}n_{36}$ fullerenes in delivery of β-lapachone anticancer drug: Dft approach. *Polyhedron*, **232**:116295, 2023. DOI: https://doi.org/10.1016/j.poly.2023.116295.

[25] M.M. Salem-Bekhit, S. Al Zahrani, N.A. Alhabib, R.R. Maaliw III, M. Da'i, and M. Mirzaei. Metal-doped fullerenes as promising drug carriers of hydroxycarbamide anticancer: Insights from density functional theory. *Chem. Phys. Impact*, **7**:100347, 2023. DOI: https://doi.org/10.1016/j.chphi.2023.100347.

[26] F.D. Prieto-Martínez, E. López-López, K.E. Juárez-Mercado, and J.L. Medina-Franco. Computational drug design methods - current and future perspectives. *In Silico Drug Des*, **2019**:19–26, 2019. DOI: https://doi.org/10.1016/B978-0-12-816125-8.00002-X.

[27] M.H. Attar Kar and M. Yousefi. Interaction of a conical carbon scaffold with the thio-substituted model of fluorouracil towards approaching the drug delivery purposes. *Main Group Chem*, **21**:725–731, 2022. DOI: https://doi.org/10.3233/MGC-210174.

[28] M.S. Sadjadi, B. Sadeghi, and K. Zare. Natural bond orbital (NBO) population analysis of cyclic thionylphosphazenes, [NSOX (NPCl2) 2]; X= F (1), X= Cl (2). *J. Mol. Struct. THEOCHEM*, **817**:27–33, 2007. DOI: https://doi.org/10.1016/j.theochem.2007.04.015.

[29] N. Kumar, P. Chamoli, M. Misra, M.K. Manoj, and A. Sharma. Advanced metal and carbon nanostructures for medical, drug delivery and bio-imaging applications. *Nanoscale*, **14**:3987–3993, 2022. DOI: https://doi.org/10.1039/D1NR07643D.

[30] R.H. Althomali, H.S. Jabbar, A.T. Kareem, B. Abdullaeva, S.S. Abdullaev, A. Alsalamy, B.M. Hussien, H.M. Balasim, and Y. Mohammed. Various methods for the synthesis of $NiTiO_3$ and $ZnTiO_3$ nanomaterials and their optical, sensor and photocatalyst potentials: a review. *Inorg. Chem. Commun*, **158**:111493, 2023. DOI: https://doi.org/10.1016/j.inoche.2023.111493.

[31] G. Chala. Review on green synthesis of iron-based nanoparticles for environmental applications. *J. Chem. Rev*, **5**:1–7, 2023. DOI: https://doi.org/10.22034/jcr.2023.356745.1184.

[32] R.H. Althomali, S.I.S. Al-Hawary, A. Gehlot, M.T. Qasim, B. Abdullaeva, I.B. Sapaev, I.H. Al-Kharsan, and A. Alsalamy. A novel Pt-free counter electrode based on MoSe2 for cost effective dye-sensitized solar cells (DSSCs): Effect of Ni doping. *J. Phys. Chem. Solid*, **182**:111597, 2023. DOI: https://doi.org/10.1016/j.jpcs.2023.111597.

[33] M. Byakodi, N.S. Shrikrishna, R. Sharma, S. Bhansali, Y. Mishra, A. Kaushik, and S. Gandhi. Emerging 0D, 1D, 2D, and 3D nanostructures for efficient point-of-care biosensing. *Biosens. Bioelectro. X*, **12**:100284, 2022. DOI: https://doi.org/10.1016/j.biosx.2022.100284.

[34] N. Gupta, K. Todi, T. Narayan, and B.D. Malhotra. Graphitic carbon nitride-based nanoplatforms for biosensors: Design strategies and applications. *Mater Today Chem*, **24**:100770, 2022. DOI: https://doi.org/10.1016/j.mtchem.2021.100770.

[35] Z.R. Al-Bahadili, A.A.S. Al-Hamdani, L.A. Al-Zubaidi, F.A. Rashid, and S.M. Ibrahim. An evaluation of the activity of prepared zinc nano-particles with extract alfalfa plant in the treatments of peptidase and ions in water. *Chem. Methodol*, **6**:522–528, 2022. DOI: https://doi.org/10.22034/chemm.2022.336588.1470.

[36] M. Taghva, S.A. Mosaddad, E. Ansarifard, and M. Sadeghi. Could various angulated implant depths affect the positional accuracy of digital impressions? An in vitro study. *J. Prosthodontics*, **7**:1–6, 2023. DOI: https://doi.org/10.1111/jopr.13764.

[37] L.S.R. Hosseini, A.M. Bazargan, F. Sharif, and M. Ahmadi. Promoting the electrical conductivity of polyimide/in-situ reduced graphene oxide nanocomposites by controlling sheet size. *Prog. Org. Coat*, **179**:107542, 2023. DOI: https://doi.org/10.1016/j.porgcoat.2023.107542.

[38] R. Esmaeilzade, K.A. Stainslavovich, M.H. Jandaghian, L.S.R. Hosseini, L.H. Saleh, and

S. Zarghampour. Correlation of structure, rheological, thermal, mechanical, and optical properties in low density polyethylene/linear low density polyethylene blends in the presence of recycled low density polyethylene and linear low density polyethylene. *Polymer Eng. Sci*, **2024**:1–7, 2024. DOI: https://doi.org/10.1002/pen.26614.

[39] S. Shaw, G.C. Shit, and D. Tripathi. Impact of drug carrier shape, size, porosity and blood rheology on magnetic nanoparticle-based drug delivery in a microvessel. *Colloids Surf. A*, **639**:128370, 2022. DOI: https://doi.org/10.1016/j.colsurfa.2022.128370.

[40] M.J. Saadh, M. Mirzaei, B.S. Abdullaeva, R.R. Maaliw III, M. Da'i, M.M. Salem-Bekhit, and R. Akhavan-Sigari. Explorations of structural and electronic features of an enhanced iron-doped boron nitride nanocage for adsorbing/sensing functions of the hydroxyurea anticancer drug delivery under density functional theory calculations. *Phys. B*, **415445**, 2023. DOI: https://doi.org/10.1016/j.physb.2023.415445.

[41] R. Das, N. Dhar, A. Bandyopadhyay, and D. Jana. Size dependent magnetic and optical properties in diamond shaped graphene quantum dots: A DFT study. *J. Phys. Chem. Solids*, **99**:34–39, 2016. DOI: https://doi.org/10.1016/j.jpcs.2016.08.004.

[42] P. Rivero, W. Shelton, and V. Meunier. Surface properties of hydrogenated diamond in the presence of adsorbates: A hybrid functional DFT study. *Carbon*, **110**:469–474, 2016. DOI: https://doi.org/10.1016/j.carbon.2016.09.050.

[43] F.Y. Alqahtani, F.S. Aleanizy, E. El Tahir, H.M. Alkahtani, and B.T. AlQuadeib. Paclitaxel. *Profiles Drug Subst. Excip. Relat. Methodol*, **44**:205–211, 2019. DOI: https://doi.org/10.1016/bs.podrm.2018.11.001.

[44] S. Zhao, Y. Tang, R. Wang, and M. Najafi. Mechanisms of cancer cell death induction by paclitaxel: An updated review. *Apoptosis*, **27**:647–652, 2022. DOI: https://doi.org/10.1007/s10495-022-01750-z.

[45] X. Xiang, X. Feng, S. Lu, B. Jiang, D. Hao, Q. Pei, Z. Xie, and X. Jing. Indocyanine green potentiated paclitaxel nanoprodrugs for imaging and chemotherapy. *Exploration*, **2**:20220008, 2022. DOI: https://doi.org/10.1002/EXP.20220008.

[46] D.L. Yu, Z.P. Lou, F.Y. Ma, and M. Najafi. The interactions of paclitaxel with tumour microenvironment. *Int. Immunopharma*, **105**:108555, 2022. DOI: https://doi.org/10.1016/j.intimp.2022.108555.

[47] M. Hashemi, M.A. Zandieh, Y. Talebi, P. Rahmanian, S.S. Shafiee, M.M. Nejad, R. Babaei, F.H. Sadi, R. Rajabi, Z.O. Abkenar, and S. Rezaei. Paclitaxel and docetaxel resistance in prostate cancer: Molecular mechanisms and possible therapeutic strategies. *Biomed. Pharma*, **160**:114392, 2023. DOI: https://doi.org/10.1016/j.biopha.2023.114392.

[48] S.N. González-Díaz, A. Canel-Paredes, A. Macías-Weinmann, O. Vidal-Gutiérrez, and R.V. Villarreal-González. Atopy, allergen sensitization and development of hypersensitivity reactions to paclitaxel. *J. Oncol. Pharm. Pract*, **29**:810–816, 2023. DOI: https://doi.org/10.1177/10781552221080415.

[49] S.D. Pennypacker, M.M. Fonseca, J.W. Morgan, P.M. Dougherty, J.R. Cubillos-Ruiz, R.E. Strowd, and E.A. Romero-Sandoval. Methods and protocols for chemotherapy-induced peripheral neuropathy (CIPN) mouse models using paclitaxel. *Methods Cell Biol*, **168**:277–282, 2022. DOI: https://doi.org/10.1016/bs.mcb.2021.12.019.

[50] Q. Yang, E. Han, S. Xu, Y. Xu, and J. Gao. Treatment of advanced ovarian cancer with carboplatin and paclitaxel in a patient undergoing hemodialysis: Case report and literature review. *Hemodial. Int*, **26**:E31, 2022. DOI: https://doi.org/10.1111/hdi.13020.

[51] D.L. Hertz, L. Chen, N.L. Henry, J.J. Griggs, D.F. Hayes, B.A. Derstine, G.L. Su, S.C. Wang, and M.P. Pai. Muscle mass affects paclitaxel systemic exposure and may inform personalized paclitaxel dosing. *British J. Clin. Pharmacol*, **88**:3222–3226, 2022. DOI: https://doi.org/10.1111/bcp.15244.

[52] J. Chan, H. Adderley, M. Alameddine, A. Armstrong, D. Arundell, R. Fox, M. Harries, J. Lim, Z. Salih, C. Tetlow, and H. Wong. Permanent hair loss associated with taxane chemotherapy use in breast cancer: A retrospective survey at two tertiary UK cancer centres. *Europ. J. Cancer Care*, **30**:e13395, 2021. DOI: https://doi.org/10.1111/ecc.13395.

[53] N. Ying, S. Liu, M. Zhang, J. Cheng, L. Luo, J. Jiang, G. Shi, S. Wu, J. Ji, H. Su, and H. Pan. Nano delivery system for paclitaxel: Recent advances in cancer theranostics. *Colloids Surf. B*, **228**:113419, 2023. DOI: https://doi.org/10.1016/j.colsurfb.2023.113419.

[54] Q. Chen, S. Xu, S. Liu, Y. Wang, and G. Liu. Emerging nanomedicines of paclitaxel for cancer treatment. *J. Control. Rel*, **342**:280–287, 2022. DOI: https://doi.org/10.1016/j.jconrel.2022.01.010.

[55] E. Jaradat, E. Weaver, A. Meziane, and D.A. Lamprou. Microfluidic paclitaxel-loaded lipid nanoparticle formulations for chemotherapy. *Int. J. Pharma*, **628**:122320, 2022. DOI: https://doi.org/10.1016/j.ijpharm.2022.122320.

[56] F. Raza, H. Zafar, M.W. Khan, A. Ullah, A.U. Khan, A. Baseer, R. Fareed, and M. Sohail. Recent advances in the targeted delivery of paclitaxel nanomedicine for cancer therapy. *Mater. Adv*, **3**:2268–2273, 2022. DOI: https://doi.org/10.1039/D1MA00961C.

[57] B. Zhao, Z. Gu, Y. Zhang, Z. Li, L. Cheng, C. Li, and Y. Hong. Starch-based carriers of paclitaxel: A systematic review of carriers, interactions, and mechanisms. *Carbohyd. Polymers*, **291**:119628–119632, 2022. DOI: https://doi.org/10.1016/j.carbpol.2022.119628.

[58] J.D. Chai and M. Head-Gordon. Long-range corrected hybrid density functionals with damped atom–atom dispersion corrections. *Phys. Chem. Chem. Phys*, **10**:6615–6619, 2008. DOI: https://doi.org/10.1039/B810189B.

[59] V.A. Rassolov, J.A. Pople, M.A. Ratner, and T.L. Windus. 6-31G* basis set for atoms K through Zn. *J. Chem. Phys*, **109**:1223–1227, 1998. DOI: https://doi.org/10.1063/1.476673.

[60] 09 Gaussian, D.01 Revision, M.J. Frisch, G.W. Trucks, H.B. Schlegel, G.E. Scuseria, M.A. Robb, J.R. Cheeseman, G. Scalmani, V. Barone, G.A. Petersson, H. Nakatsuji, X. Li, M. Caricato, A. Marenich, J. Bloino, B.G. Janesko, R. Gomperts, B. Mennucci, H.P. Hratchian, J.V. Ortiz, A.F. Izmaylov, J.L. Sonnenberg, D. Williams-Young, F. Ding, F. Lipparini, F. Egidi, J. Goings, B. Peng, A. Petrone, T. Henderson, D. Ranasinghe, V.G. Zakrzewski, J. Gao, N. Rega, G. Zheng, W. Liang, M. Hada, M. Ehara, K. Toyota, R. Fukuda, J. Hasegawa, M. Ishida, T. Nakajima, Y. Honda, O. Kitao, Nakai H., T. Vreven, K. Throssell, J.A. Montgomery, Jr., J.E. Peralta, F. Ogliaro, M. Bearpark, J.J. Heyd, E. Brothers, K.N. Kudin, V.N. Staroverov, T. Keith, R. Kobayashi, J. Normand, K. Raghavachari, A. Rendell, J.C. Burant, S.S. Iyengar, J. Tomasi, M. Cossi, J.M. Millam, M. Klene, C. Adamo, R. Cammi, J.W. Ochterski, R.L. Martin, K. Morokuma, O. Farkas, J.B. Foresman, and D.J. Fox. . *Gaussian, Inc, Wallingford CT*, **21**:2133–2148, 2009. URL https://www.gaussian.com.

[61] N. Alfryyan, M. Sohail, N. Rahman, O.H. Alsalmi, A. Ullah, A.A. Khan, M.S. Al-Buriahi, Z.A. Alrowaili, and B.S. Abdullaeva. First-principles calculations to investigate structural, electrical, elastic and optical characteristics of BWF_3 (W= S and Si) fluoroperovskites. *Results Phys*, **52**:106812–106818, 2023. DOI: https://doi.org/10.1016/j.rinp.2023.106812.

[62] M.N. Sidik, Y.M. Bakri, S.S.S.A. Azziz, A.K.O. Aldulaimi, C.F. Wong, and M. Ibrahim. In silico xanthine oxidase inhibitory activities of alkaloids isolated from Alphonsea sp. *South Afric. J. Botany*, **147**:820–825, 2022. DOI: https://doi.org/10.1016/j.sajb.2022.03.024.

[63] T. Lu and F. Chen. Multiwfn: a multifunctional wavefunction analyzer. *J. Comput. Chem*, **33**:580–586, 2012. DOI: https://doi.org/10.1002/jcc.22885.

[64] P.L. Popelier. The QTAIM perspective of chemical bonding. *Chem. Bond*, **2014**:271–276, 2014. DOI: https://doi.org/10.1002/9783527664696.ch8.

[65] B. Mennucci. Polarizable continuum model. *Wiley Interdisciplin. Rev. Comput. Mol. Sci*, **2**:386–341, 2012. DOI: https://doi.org/10.1002/wcms.1086.

[66] M. Gutowski, J.H. Van Lenthe, J. Verbeek, F.B. Van Duijneveldt, and G. Chałasinski. The basis set superposition error in correlated electronic structure calculations. *Chem. Phys. Lett*, **124**:370–376, 1986. DOI: https://doi.org/10.1016/0009-2614(86)85036-9.

[67] Y. Huang, C. Rong, R. Zhang, and S. Liu. Evaluating frontier orbital energy and HOMO/LUMO gap with descriptors from density functional reactivity theory. *J. Mol. Model*, **23**:3–7, 2017. DOI: https://doi.org/10.1007/s00894-016-3175-x.

[68] A. Saedi, A. Mashinchian Moradi, S. Kimiagar, and H.A. Panahi. Photosensitization of fucoxanthin-graphene complexes: a computational approach. *Main Group Chem*, **21**:1065–1071, 2022. DOI: https://doi.org/10.3233/MGC-210188.

[69] M. Da'i, M. Mirzaei, F. Toiserkani, S.M. Mohealdeen, Y. Yasin, M.M. Salem-Bekhit, and R. Akhavan-Sigari. Sensing the formaldehyde pollutant by an enhanced BNC18 fullerene: DFT outlook. *Chem. Phys. Impact*, **7**:100306–100311, 2023. DOI: https://doi.org/10.1016/j.chphi.2023.100306.

[70] F. Toiserkani, M. Mirzaei, V. Alcan, K. Harismah, and M.M. Salem-Bekhit. A facile detection of ethanol by the Be/Mg/Ca-enhanced fullerenes: Insights from density functional theory. *Chem. Phys. Impact*, **7**:100318–100322, 2023. DOI: https://doi.org/10.1016/j.chphi.2023.100318.

[71] Chemcraft Version 1.8 and build 682. Graphical software for visualization of quantum chemistry computations. *Chemcraftprogaram*, . URL https://www.chemcraftprog.com.

[72] N.M. O'boyle, A.L. Tenderholt, and K.M. Langner. Cclib: A library for package independent computational chemistry algorithms. *J. Comput. Chem*, **29**:839–846, 2008. DOI: https://doi.org/10.1002/jcc.20823.

[73] R. Peyab, S. Hosseini, and M.D. Esrafili. Al- and Ga-embedded boron nitride nanotubes as effective nanocarriers for delivery of rizatriptan. *J. Mol. Liq*, **361**:119662, 2022. DOI: https://doi.org/10.1016/j.molliq.2022.119662.

[74] F. Nattagh, S. Hosseini, and M.D. Esrafili. Effects of B and N doping/codoping on the adsorption behavior of C60 fullerene towards aspirin: A DFT investigation. *J. Mol. Liq*, **342**:117459, 2021. DOI: https://doi.org/10.1016/j.molliq.2021.117459.

[75] F. Ghazali, S. Hosseini, and S. Ketabi. DFT and molecular simulation study of gold clusters as effective drug delivery systems for 5-fluorouracil anticancer drug. *J. Cluster Sci*, **34**:1499–1505, 2023. DOI: https://doi.org/10.1007/s10876-022-02329-z.

[76] F.D. Prieto-Martínez, E. López-López, K.E. Juárez-Mercado, and J.L. Medina-Franco. Computational drug design methods - current and future perspectives. *In Silico Drug Design*, **2**:19–25, 2019. DOI: https://doi.org/10.1016/B978-0-12-816125-8.00002-X.